ESR study of the Kondo effect in Au^{171} Yb and Au^{174} Yb

Y. von Spalden, E. Tsang,* and K. Baberschke
Institut für Atom- und Festkörperphysik, Freie Universität Berlin, Arnimallee 14, D-1000 Berlin 33, Federal Republic of Germany

P. Schlottmann
Institut für Festkörperforschung, Kernforschungsanlage Jülich, Postfach 1913, D-5170 Jülich, Federal Republic of Germany
(Received 22 December 1982)

Recently we have reported on Kondo anomalies in the g-value shift and the relaxation rate of ESR in *Au*Yb. This work was extended (1) to a low Yb concentration of 70 ppm to avoid interaction effects and (2) to 1-GHz experiments, in addition to those at 3 and 9 GHz, to study frequency and magnetic field effects. Experiments were performed down to 80 mK ($\hbar\omega \gtrsim kT$). We present a theoretical analysis of the longitudinal and transverse dynamic susceptibilities, taking into consideration the finite field and frequency. This analysis is based on the work of Götze and Wölfle, and agrees well with the experiments and shows in particular that in the g-value shift the frequency and field dependence is less important than for the relaxation. The only fit parameter for all relaxation data (different isotopes, concentrations, frequencies, and fields) is the Kondo temperature T_K. The theoretical fit explains the relaxation data quite well; however, the fit of the g-value shift yields a different T_K.

I. INTRODUCTION

The paramagnetic resonance of very dilute alloys provides us with detailed information on the exchange interaction of a single impurity and the conduction electrons (CE's) of the host metal. It has been suggested already for a long time to detect higher-order corrections in this interaction, namely the Kondo effect, by means of the ESR technique.

The Kondo effect should show up in the g-value shift[1] and the relaxation rate. The relaxation divided by temperature is not a constant anymore, but shows a logarithmic increase when lowering the temperature. That twofold and independent appearance of the same effect in one experiment favors the ESR technique. Most of the other experiments detect only one contribution, either the static or dynamic local susceptibility, i.e., for *Cu*Fe quasielastic neutron scattering[2] determines the relaxation and Mössbauer effect[3] determines the change in the hyperfine field ($\sim\chi^{\text{static}}$).

One exception is the NMR of *Cu*Mn, where Alloul[4] has detected both effects also. A limitation for investigating the Kondo effect by ESR is that the maximum linewidth is of the order of the Kondo temperature: $\Delta H_{\min} \cong (4/3\pi) T_K$.[5] For $\Delta H_{\min} \cong 100$ G, one gets a T_K of a few millikelvins. As a consequence, all ESR are limited to the regime of $T \gg T_K$.

In addition, most of the physical Kondo systems, known from resistivity work, for example, are not suitable for ESR for the following reasons: $3d$ impurity ions such as Cr, Fe, and Co have never been detected in a local-moment (single-ion) resonance, the spin-flip rate being too large: $\tau_{\text{sf}}^{-1} \gtrsim \omega_{\text{Larmor}}$. Mn in Cu is completely bottlenecked, that is to say, the moderate strong exchange coupling between local moment and CE's does not show up in an ESR experiment.[6] We are left with $4f$ systems. Since Ce is not suitable because of its instable-moment character, only Yb remains as a local-moment candidate. In *Au*Yb, a local $4f^{13}$ state is formed (*Ag*Yb is diamagnetic). After the first detection of the negative g-value shift in *Au*Yb (Ref. 7), the resistivity minimum has been detected as well.[8] Recently, Baberschke and Tsang[9] (BT) detected, by means of low-T ($T < 1$ K) and low-frequency ESR, the $\ln T$ in the relaxation, yielding a Kondo temperature on the order of microkelvins.

The purpose of the present work is the following.

(1) To present more complete experiments ranging down to $T \cong 80$ mK and to concentrations of only $c \cong 70$ ppm Yb. The use of a dilution refrigerator, which cools the sample only, allows us to change the microwave frequencies from 1 to 9 GHz without warming up the sample. With respect to its flexibility, the setup represents a unique experimental facility.[10] As we will show, the use of different microwaves is crucial because finite microwave frequencies ($\hbar\omega \gtrsim kT$) and/or applied magnetic fields influence the relaxation rates and the g-value shift.

(2) We use different isotopes, namely ^{174}Yb to avoid hyperfine fields and ^{171}Yb to study its effects. It is known that hyperfine structure (hfs) influences the Kondo effect.[11]

(3) The higher precision of our present data with respect to BT allows us to discuss in more detail the theoretical analysis, namely the magnetic field and (independently) the frequency effects. The calculations by Götze and Wölfle[5] seem to be the most adequate. The results are compared with the Mössbauer work.[12]

For brevity in this paper we will avoid a repetition of current formulas. Our notation is consistent with Refs. 6, 9, etc., i.e., $\hat{H}_{\text{ex}} = -J\vec{S}\cdot\vec{s}$, J_0 is the bare exchange integral, $J_{\text{eff}}(T)$ is the effective exchange interaction relevant at T

[Ref. 9(a)], and T_1^{-1} and T_1^{-1} are the longitudinal and transverse relaxation rates.

II. EXPERIMENTAL RESULTS

Master alloys of ^{174}Yb and ^{171}Yb were prepared by arc melting. From these alloys, samples with lower concentrations of Yb were prepared. The growing of single crystals, cutting, and etching are described in Ref. 13.

The sample concentration was determined from saturation magnetization measurements at $T=1.6$ K and fields up to $H=50$ kG, showing a concentration gradient over the length of the samples between 9% and 20%.[13] The ESR experiments were performed in a bath cryostat and a ^{3}He-^{4}He dilution refrigerator.[10] With respect to Ref. 10, we have reduced the diameter of the quartz-glass fingers, the outer one having a cross-sectional diameter of 24 mm. This allows us to switch rapidly between microwave units for 1.1, 3.4, 4.1 (Bruker), and 9.0 GHz (Varian), since all cavities have 1-in. sample holes.

The microwave power we can use in the very-low-temperature regime is quite small due to the limited cooling power of the ^{3}He-^{4}He dilution refrigerator. For comparison, we will give the microwave power P_{MW} used to produce the same heating at low temperatures (from $T=84$ mK at $P_{MW}=0$ to $T=100$ mK for power given): $P_{MW}=50$ μW at 9.0 GHz, $P_{MW}=330$ μW at 3.4 GHz, and $P_{MW}=2.1$ mW at 1.1 GHz. This means, since only a small fraction of this power is actually absorbed by the eddy currents in the sample, that the lower sensitivity of the 3.4- and 1.1-GHz equipment can partly be compensated by a larger microwave power. Power levels actually used for recording spectra from which data were extracted were $P_{MW}=20$ μW at $T=89$ mK and 9 GHz and $P_{MW}=330$ μW at $T=84$ mK and 1.1 GHz. This results in negligible heating due to the applied microwave. At higher temperatures, the cooling power of the dilution refrigerator increases, allowing us to use higher power levels without heating the sample by the microwave: $P_{MW}=300$ μW at $T=980$ mK and 9.0 GHz, $P_{MW}=912$ μW at $T=950$ mK and 3.4 GHz.

It is also important to keep the low-frequency field modulation small in order to avoid heating. Here we used the same modulation frequency of 25 kHz for all cavities.

The lower sensitivity of the lower-frequency microwave bridges is in part also compensated by a smaller residual linewidth a, giving a narrower experimental linewidth. Additionally, the skin depth is larger at lower frequency. Using pure ^{174}Yb isotope with zero nuclear spin gives an additional 30% intensity as compared to natural abundance Yb.

In the dilution refrigerator, a calibrated resistor located on the outside of the mixing chamber was used to measure the temperature. Figure 1(a) shows a typical spectrum for 1.1 GHz, the lowest concentration of $c=70$ ppm at $T=100$ mK. In this case the microwave power was $P_{MW}=330$ μW. However, the ESR technique itself allows one to determine the temperature of the sample independently via the Boltzmann population as can be seen in Fig. 2. In our experiments the intensity ratio of the two hyperfine lines of the Au ^{171}Yb ($I=\frac{1}{2}$) samples was used to control the temperature. Comparison with the temperature indicated by the resistance thermometer showed fair agreement, as shown in the inset of Fig. 2. At a temperature of $T=1.51$ K, the two hyperfine levels are equally populated, while at $T=105$ mK the high-field transition ($m_I=-\frac{1}{2}$) has a weaker intensity. Similar arguments have been used in previous AuEr (Refs. 14 and 15) experiments.

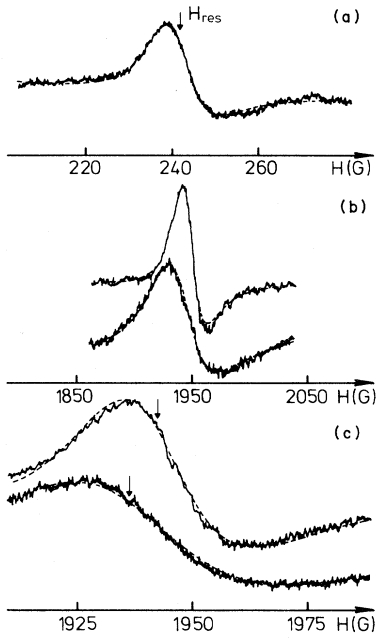

FIG. 1. (a) Recorder trace of a $c=70$-ppm Au ^{174}Yb sample at $T=100$ mK and $f=1.122$ GHz. The fit (dashed line) yields $\Delta H=9.8\pm0.5$ G and $H_{res}=2.242.4\pm0.6$ G. For error bar see text. (b) and (c) are the same as (a), but at $f=9.005$ GHz, (b) spectra are at 400-G scan range, and (c) spectra are at 100-G scan range. The upper curves in (b) and (c) were recorded at $T=89$ mK, the lower ones at $T=605$ mK. The fit yields at $T=89$ mK, $\Delta H=23.4\pm1$ G, $H_{res}=1943.5\pm2$ G, and at $T=605$ mK, $\Delta H=40.3\pm2$ G and $H_{res}=1957.6\pm3$ G (dashed lines).

Since we want to determine small changes in H_{res} and in the linewidth ΔH, a precise determination of both parameters is necessary. Conventional techniques following the pioneer work of Peter *et al.*[16] or other parameter fits would be inadequate. One needs to fit the full line shape. This has been done by a simple simulation of a Lorentzian line and its dispersion part to get a Dysonian[17] line shape (we use the formula of Hacker *et al.*[18]). Figure 1 shows that, within the noise level of the experiment, the fits agree almost perfectly. A parameter to be determined is the ratio of the superposition of the absorption and dispersion part: $b\chi'+\chi''$. This parameter b equals 1 in the dirty limit ($b=1$) if one follows the Dysonian theory. In all our experiments of dilute Au samples, that is to say AuGd (Ref. 19), AuEr,[13] and previous AuYb (Ref. 9) experiments, we had to use $b=0.8$. We attribute this to the high conductivity of Au single crystals. The figure

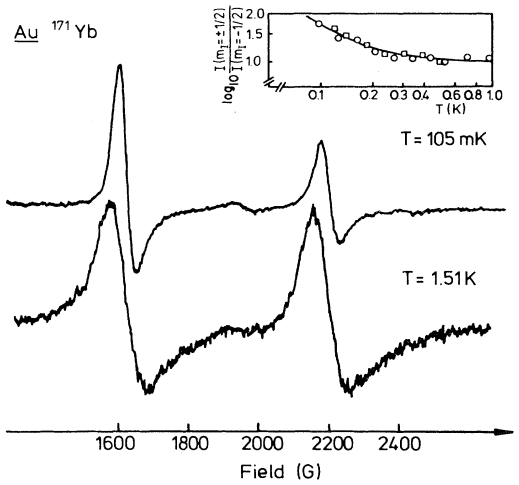

FIG. 2. Recorder trace of a $c=670$-ppm *Au* ^{171}Yb sample at $f=8.995$ GHz. The inset shows the intensity ratio of the two hf transitions for the $c=280$ ppm (□) and $c=670$ ppm (○).

$b=0.8$ was taken absolutely fixed and therefore does not enter as an uncertainty for $H_{\rm res}$ or ΔH.

In Figs. 1(b) and 1(c) we show for the same sample four spectra which were recorded at $f=9.0$ GHz and $T=89$ and 605 mK, respectively. The two top (89-mK), respectively, bottom (605-mK) spectra in Figs. 1(b) and 1(c) differ only in the scan range used: First, the spectrum with a 400-G scan in Fig. 1(b) was recorded, then, staying at the same temperature, the spectrum in Fig. 1(c) was recorded with a 100-G sweep. This technique was used recording all our spectra [Fig. 1(a) also] because it allowed us to determine the field for resonance and the experimental linewidth with a higher precision than in our previous experiments.[9] In addition, we did control on line the applied field and the microwave frequency with the necessary precision. In the following we will present the experimental results for the *Au* ^{174}Yb and *Au* ^{171}Yb samples.

A. *Au* ^{174}Yb

Since the ^{174}Yb isotope has zero nuclear spin ($I=0$), only one line is observed. The line shape of this resonance is therefore not distorted by hyperfine (hf) transitions of isotopes with $I=\frac{1}{2}$ and $I=\frac{5}{2}$. Only a single line fit is necessary as compared with a multiline fit for natural abundance Yb. Figure 3 shows the g values as a function of temperature on a linear-T scale. Compared to Fig. 2 of Ref. 9(a), the data scatter is reduced significantly. The main feature of this diagram, the decreasing g value at decreasing temperature, is clearly visible. The error bars given are relative errors, which are larger for higher temperatures because of the larger experimental linewidth. The absolute error bar for the g value is $\delta g=\pm 0.005$. For the 1.1-GHz resonance [see Fig. 1(a)], the error in the field for resonance is roughly 2 times larger. Therefore we give no data of the g value for these experiments.

In determining the relaxation part of the experimental linewidth, one has to determine the residual linewidth a: $\Delta H_{\rm exp}=\Delta H_{\rm rel}+a$. This is done by plotting all experimen-

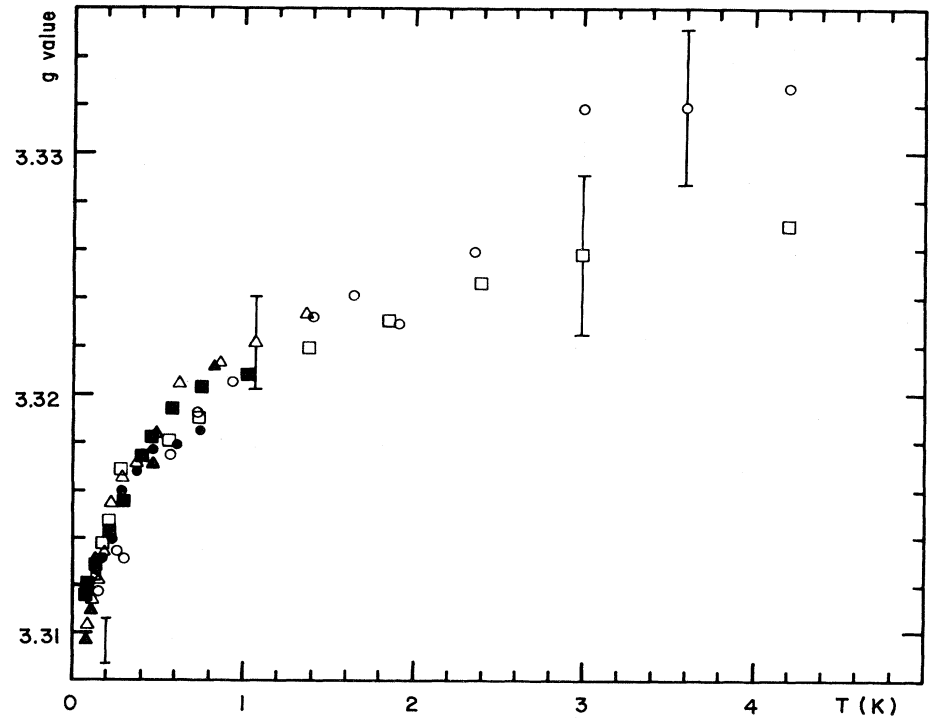

FIG. 3. g values for the *Au* ^{174}Yb samples: △, 9.0 GHz, 70 ppm; □, 9.0 GHz, 200 ppm; ○, 9.0 GHz, 260 ppm; ▲, 3.4 GHz, 70 ppm; ■, 3.4 GHz, 200 ppm; ●, 3.4 GHz, 260 ppm (the 260-ppm sample is a natural abundance Yb sample).

TABLE I. Residual linewidth data for the *Au* ^{174}Yb and *Au* ^{171}Yb samples. The error bars are absolute. The 200-ppm sample has excessive residual linewidth at 9.0 GHz due to mechanical mistreatment prior to the measurement.

Au ^{174}Yb	Residual linewidth a (G)			*Au* ^{171}Yb	Residual linewidth a (G)	
f (GHz)	$c=70$ ppm	$c=200$ ppm	$c=260$ ppm	f (GHz)	$c=280$ ppm	$c=670$ ppm
9.0	15.5±0.80	20.0±1.0^{+}	19.8±1.0	9.0	21.0±1.0	32.0±1.6
3.4	8.5±0.45	8.9±0.45	11.5±0.60	3.4	13.5±0.70	
1.1	4.0±0.20			1.1	10.7±0.55	

tal linewidth data for a given sample on a linear-T scale. Extrapolation of the high-temperature data ($T>1.5$ K) (where the influence of finite magnetic field and microwave frequency is small) to $T=0$ gives the residual linewidth a. These residual linewidths for each experiment are not uncorrelated values. As has been previously shown, a is both concentration and frequency dependent[13]: $a=\alpha c+\beta f+\gamma cf$. Thus by using different microwave frequencies and different concentrations, one has a set of correlated residual linewidth data. Table I gives the values for a of both ^{174}Yb and ^{171}Yb and their absolute error bars (for details, see Ref. 13). The relevant quantity to be discussed is the relaxation per temperature $(\Delta H_{\text{exp}}-a)/T$ as a function of $\ln T$. One cannot extrapolate a precisely enough from high T. Therefore we did allow a small feedback on the parameter a (typically less than 5% of a) to improve the agreement between experimental data and theory in the very-low-temperature regime. Figure 4 shows the relaxation rate W: $\hbar W=g(\Gamma_7)\mu_B(\Delta H-a)$, divided by temperature for the ^{174}Yb isotope on a $\ln T$ scale for the three microwave frequencies used. For comparison, the Mössbauer data of *Au* ^{170}Yb of Ref. 20 are also shown. The theoretical curves (solid lines) will be discussed in Sec. III.

B. *Au* ^{171}Yb

The energy-splitting scheme as a function of the applied magnetic field for the ^{171}Yb isotope is shown in Fig. 5. The vertical arrows indicate the possible transitions for the three microwave frequencies of 1.1, 3.4, and 9.0 GHz. The dashed lines show, in addition, the energy levels and transitions for the ^{174}Yb isotope. At 1.1 GHz we only observed the hf transition at a magnetic field $H=370$ G, we

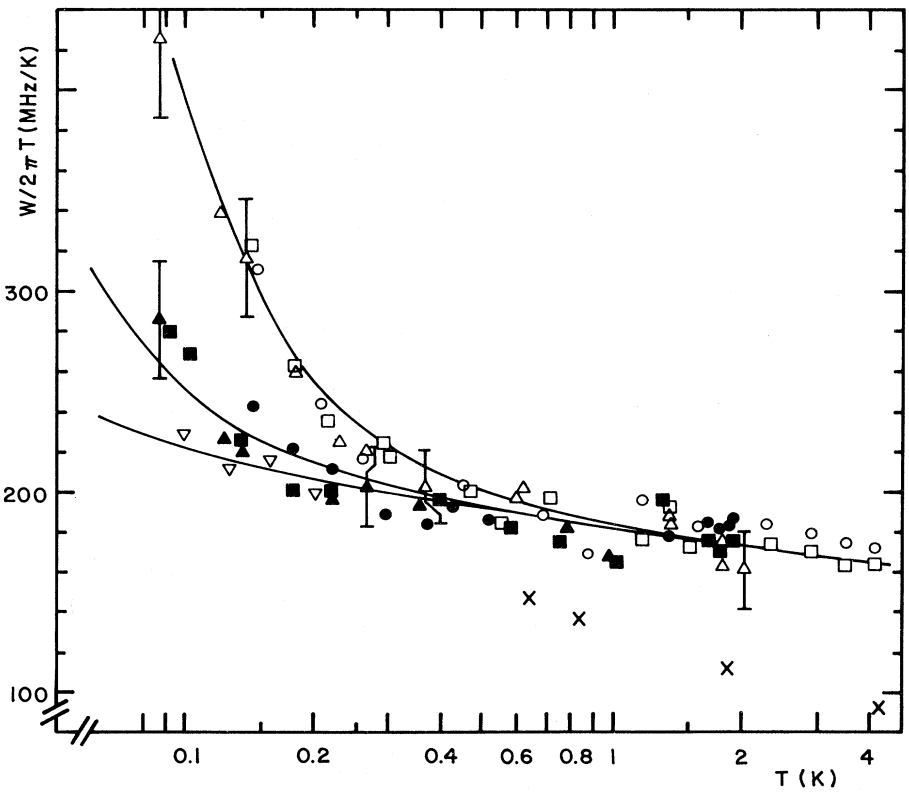

FIG. 4. Relaxation per temperature for the *Au* ^{174}Yb samples: △, 9.0 GHz, 70 ppm; □, 9.0 GHz, 200 ppm; ○, 9.0 GHz, 260 ppm; ▲, 3.4 GHz, 70 ppm; ■, 3.4 GHz, 200 ppm; ●, 3.4 GHz, 260 ppm; ▽, 1.1 GHz, 70 ppm (the 260-ppm sample is a natural abundance Yb sample). For comparison, the Mössbauer data of Ref. 20 are also given (×).

were not able to detect the nuclear transition at $H \cong 1.1$ kG. We obtained the best fit for all experiments in choosing $A = 579.0 \pm 2$ G. However, this error is in the order of 3×10^{-3}. This is not sufficient to calculate H_{res} in higher order (relevant for g) with a precision as high as for ^{174}Yb. The g value agrees with $g(^{174}\text{Yb})$, and the hf coupling constant with the literature data.[21] The disadvantage of less precision in g is compensated by (1) the fact that two lines ($2 \times \Delta H_{exp}$) at different applied fields are detected, and (2) one can use the relative intensities to check the temperature of the sample (Fig. 2).

It is worthwhile to mention that the effect of the hf field on the Kondo effect[11] cannot be detected so easily in the ^{174}Yb and ^{171}Yb ESR. For all three resonances ^{174}Yb and $I=0$, ^{171}Yb and $m_I = -\frac{1}{2}$, and $m_I = +\frac{1}{2}$, the local field seen by the $4f$ moment ($H_{hf} + H_{ext}$) is always the same.

To determine the relaxation part of the experimental linewidth we follow the same procedure as for the ^{174}Yb isotope. However, for each temperature one has two experimental values, one for the low-field hf transition ($m_I = +\frac{1}{2}$) and one for the high-field hf transition ($m_I = -\frac{1}{2}$).

Since the microwave frequency and the magnetic field at the ion's site at resonance are equal, so is the residual linewidth (Table I). The values of the relaxation rate divided by temperature versus a $\ln T$ scale are shown in Fig. 6 together with the theoretical fits.

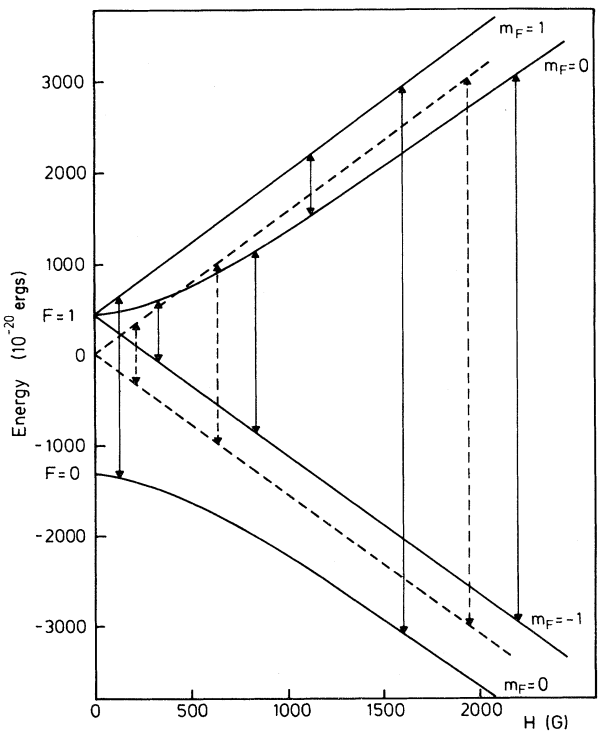

FIG. 5. Energy-splitting scheme for the ^{171}Yb ($I = \frac{1}{2}$) isotope. The possible transitions for the three microwave frequencies of 1.1, 3.4, and 9.0 GHz are indicated by the vertical arrows. Dashed lines give energy levels and transitions for the ^{174}Yb ($I=0$) isotope.

Both Figs. 4 and 6 have in common that the relaxation divided by temperature is not a constant value, but increases at decreasing temperature. Above $T = 1$ K, there is no detectable difference in the relaxation rate between different microwave frequencies (see figure captions for explanation of symbols). Below $T = 0.3$ K, however, clear differences between the microwave frequencies can be seen. At 1.1 GHz, for both the ^{174}Yb (∇) and ^{171}Yb isotope (●), one sees almost a perfect $\ln T$ dependence of the relaxation rate. At 3.4 GHz, the relaxation rate increases more at lower temperatures as compared to 1.1 GHz. The 9.0-GHz data show the highest relaxation rate in this low-temperature regime. The error bars given are relative errors of the experimental linewidth plus errors in the temperature.

III. ANALYSIS

In the previous analysis (BT) we have employed the simple model of an effective (temperature-dependent) exchange[22,23] yielding

$$\Delta g = \alpha d \mid \ln(T_K/T) \mid^{-1}, \qquad (1)$$
$$\delta_{ie}/\pi k T = \alpha^2 d \mid \ln(T_K/T) \mid^{-2},$$
$$T_K = D \exp[1/N(E_F)J_0]$$

where α takes into consideration the projection of $\vec{S}$ on $\vec{J}$, $\alpha = (g_J - 1)g_J^{-1} g_{eff} = 0.418$ for Γ_7 Yb, and d weighs the degeneracy $d = (2l+1)$. The effect of a finite magnetic field on the relaxation and the g-value shift is ignored. The difference in the longitudinal and transverse relaxation T_1^{-1} and T_2^{-1} and its exact formulas for $\hbar\omega \approx kT$ is neglected, too.

In the present analysis we calculated the longitudinal and transverse dynamical impurity-spin susceptibilities, following Götze and Wölfle.[5] The longitudinal susceptibility yields T_1^{-1} which is a spin-flip rate. The transverse susceptibility yields T_2^{-1}. This relaxation in presence of an applied magnetic field is in part due to $S_z s_z$ terms and can be seen as a "frequency modulation" term or a phase memory time. The Mössbauer experiment detects only T_1^{-1}. In the absence of a magnetic field and for cubic symmetry one gets $T_1^{-1} = T_2^{-1}$. Consequently, in this limit one expects $T_{ESR}^{-1} = 2T_{Me}^{-1}$. Figure 6 shows that the experiment yields $1 < T_{ESR}^{-1}/T_{Me}^{-1} < 2$.

In order to calculate the dynamical susceptibilities for our particular system AuYb and for the temperature range $T_K \ll T < 4$ K, we made the following assumptions.

(i) Only the $4f^{13}$ configuration plays a role.

(ii) Only the $j = \frac{7}{2}$ Hund's-rule ground state enters.

(iii) We neglect admixture of the excited Γ_6 and Γ_8 crystal-field levels into the Γ_7 ground state and assume T, H, ω to be smaller than crystalline electric field (CEF) splitting.

(iv) Since H is much smaller than CEF we neglect the Van Vleck admixture of the Γ_8 into the Γ_7 doublet.[24]

(v) Hybridization is small compared to $E_0 = E_F - E(\Gamma_7)$ and CEF splitting (Δ) is much smaller than E_0. Anisotropy of the exchange coupling is then small (Δ/E_0 times smaller than the isotropic part) and is neglected.[25]

Points (iii)–(v) imply that we do not deal with anisotropic

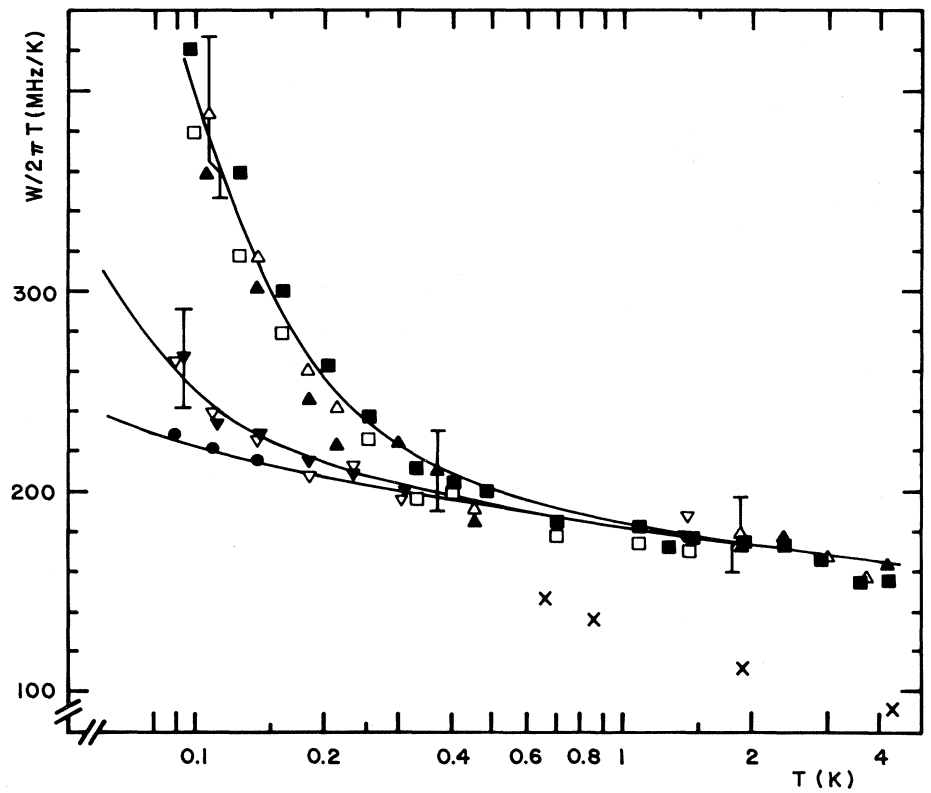

FIG. 6. Relaxation per temperature for the Au^{171}Yb samples. Open symbols denote the $m_I=+\frac{1}{2}$ transitions, closed symbols denote the $m_I=-\frac{1}{2}$ transitions: △ and ▲, 9.0 GHz, 280 ppm; □ and ■, 9.0 GHz, 670 ppm; ▽ and ▼, 3.4 GHz, 280 ppm; ●, 1.1 GHz, 280 ppm.

exchange parameters as J_{01}, J_{11}, etc. We do not have a thermal population of Γ_8 as in the Mössbauer work[25] for higher T, nor do we apply large magnetic fields as in NMR.[24]

With the above assumptions and restrictions the model is equivalent to a spin-$\frac{1}{2}$ s-d model with an effective magnetic moment of $\mu=g(\Gamma_7)\mu_B$, since

$$|\Gamma_7,\sigma\rangle=(\tfrac{3}{4})^{1/2}|\sigma,\tfrac{5}{2}\rangle-\tfrac{1}{2}|-\sigma,\tfrac{3}{2}\rangle$$
$$=|\sigma\rangle,\quad \sigma=\pm 1\ .$$

The Schrieffer-Wolff transformation yields the following (Coqblin and Schrieffer[26]) with $S_z=\frac{1}{2}\sum_\sigma \sigma|\sigma\rangle\langle\sigma|$ and $S^+=|+\rangle\langle-|$:

$$\hat{H}_0=\sum_{k,\sigma}E_k c^\dagger_{k\sigma}c_{k\sigma}-h_0 S_z\ ,$$
$$\hat{H}_{\rm ex}=-2J\sum_{k,k',\sigma,\sigma'}\vec{\mathbf{S}}\cdot c^\dagger_{k\sigma}\vec{s}_{\sigma\sigma'}c_{k'\sigma'}-\frac{J}{2}\sum_{k,k',\sigma}c^\dagger_{k\sigma}c_{k'\sigma}\ , \tag{2}$$

where $s^i_{\sigma\sigma'}$ are the spin-$\frac{1}{2}$ Pauli matrices. The last term is a normal scattering and irrelevant for magnetism.

We first self-consistently calculated the effective field h for a given h_0 (Ref. 27) in leading logarithmic order:

$$\Delta g/g_0=(2\{\ln(T_K/T)+\Psi(1)-\mathrm{Re}\Psi[1-ih/(2\pi T)]\})^{-1}\ ,$$
$$h=(1+\Delta g/g_0)h_0\ , \tag{3}$$

where Ψ denotes the digamma function. The only parameter which enters is h_0 or $\hbar\omega$. As the ionic g value we choose g_0 (ThO_2)=3.423 (for details see Sec. IV). Equation (3) was fitted to the experimental data (Fig. 7) by varying T_K. The solid lines show the best fit and demonstrate that the magnetic field or frequency effect is very small. The experimental data do not differ between 9 (open symbols) and 3.4 GHz (closed symbols) within the error bars. Note for the way of analysis we do have only one fit parameter T_K, a change in T_K shifts the solid lines *and* changes the slopes. For comparison, we show a fit using Eq. (1) (dashed line).

Before we discuss the problems of such a fit procedure we first continue in the analysis of the linewidth. The longitudinal and transversal susceptibilities can be calculated by introducing the relaxation kernels $N_L(z)$ and $N_T(z)$ (Ref. 5):

$$\chi_L(z)=\frac{N_L(z)}{z+N_L(z)/\chi_0^L}\ ,$$
$$\chi_T(z)=\frac{N_T(z)-\frac{1}{2}\tanh(h/2T)}{z-h+N_T(z)/\chi_0^T}\ , \tag{4}$$

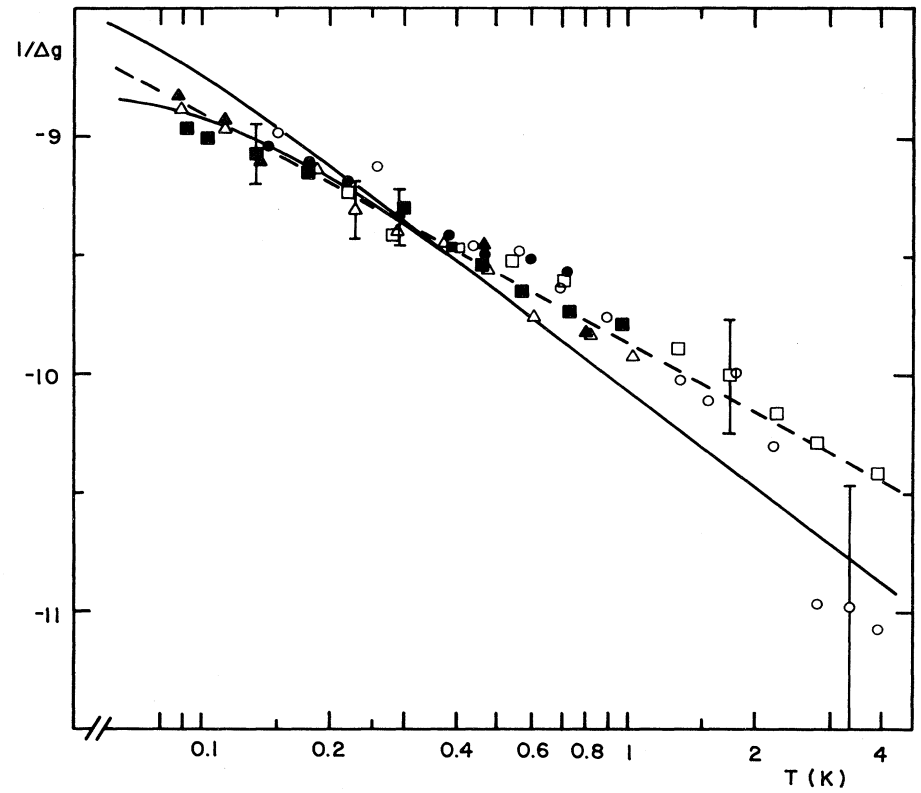

FIG. 7. $1/g$-value shift as a function of temperature for the ^{174}Yb samples. We used for $g(\Gamma_7)$ the value in ThO_2:$g=3.423$: △, 9.0 GHz, 70 ppm; □, 9.0 GHz, 200 ppm; ○, 9.0 GHz, 70 ppm; ▲, 3.4 GHz, 70 ppm; ■, 3.4 GHz, 200 ppm; ●, 3.4 GHz, 260 ppm (the 260-ppm sample is a natural abundance Yb sample). Solid lines are theoretical curves for $T_K=4\times10^{-8}$ K and 3.4 and 9.0 GHz, respectively. The dashed line is the theoretical curve as in the previous analysis (BT) with $T_K=6\times10^{-11}$ K and $d=5.6$.

where

$$\chi_0^L=(1+\Delta g/g_0)^2\{4T\cosh^2[h/(2T)]\}^{-1}$$

and

$$\chi_0^T=(1+\Delta g/g_0)\tanh[h/(2T)]/(2h_0)$$

are the static susceptibilities. By extending Ref. 5, the relaxation kernels are evaluated in leading logarithmic order:

$$N_L(\omega)=-[(\omega-h)/2\omega]\tanh(h/2T)[\phi(\omega-h)-\phi(-h)]+(i\pi/8)\frac{\tanh(h/2T)}{(h/2T)}\phi^2(\omega-h)+(h\to-h)\ , \tag{5a}$$

$$N_T(\omega)=-[(\omega-h)/2\omega]\tanh(h/2T)[\phi(\omega-h)-\phi(-h)]+(i\pi/8)\left[1+\frac{\tanh(h/2T)}{(h/2T)}\right]\phi^2(\omega-h)\ , \tag{5b}$$

where

$$\phi(\omega)=\{\ln(T_K/T)-\tfrac{1}{2}\psi[1-i(\omega)/2\pi T]-\tfrac{1}{2}\psi(1-ih/2\pi T)\}^{-1}\ .$$

According to Ref. 5, we expand N_L around $\omega=0$ and N_T around $\omega=h$:

$$N_L(\omega)=i\Delta_L+\gamma_L\omega,\quad \omega \text{ small}$$

$$N_T(\omega)=i\Delta_T+\gamma_T(\omega-h),\quad \omega-h \text{ small}\ .$$

The relaxation rates are then given by

$$T_1^{-1}=\Delta_L/(\chi_0^L+\gamma_L)\ ,$$
$$T_2^{-1}=\Delta_T/(\chi_0^T+\gamma_T)\ . \tag{6}$$

The above results are valid if $T\gg T_K$.

The solid lines in Figs. 4 and 6 show the best fit of $W=T_1^{-1}+T_2^{-1}$. All six curves are calculated with one Kondo temperature; the agreement for both isotopes and the three frequencies are surprisingly good. We wish to point out the two, in principle, different and independent contributions, which result in an increasing relaxation at low T: (i) The Kondo effect is a result of third-order perturbation theory. This can be seen most clearly in the lowest curves (1 GHz) in Figs. 4 and 6. (ii) An effect

TABLE II. Kondo temperatures from different fits, BT, see Eq. (1). $g=3.423$.

	BT	This work
g-value shift	$T_K=6\times10^{-11}$ K $d=5.6$	$T_K=4\times10^{-8}$ K
Relaxation	$T_K=10^{-5}$ K $d=4.9$	$T_K=2\times10^{-12}$ K

which appears already in first Born approximation and for Gd or Er in Au as well; it is the finite longitudinal relaxation T_1^{-1} at a finite frequency in the limit of $h\omega > kT$ [Eq. (3) in BT].

The latter seems to be even larger than the former contribution at $T\approx100$ mK. A more detailed analysis of Eqs. (4)—(6) shows that the latter depends also on T_K. There is a cross play between the two.

The best fit for all data yields $T_K=2\times10^{-12}$ K, see Table II. This seems to be quite unsatisfactory, because $T_K^{\Delta g}$ and T_K^{relax} differ by almost 4 orders of magnitude and both are very small. The latter point is not in conflict with other experiments. Only upper limits ($T_K<1$ mK) were given in the literature.[25] The T_K in BT is larger because of experimental uncertainty (see scatter in Table I of BT). Note that all results depend only logarithmically on T_K. At first glance the former statement $T_K^{\Delta g}\neq T_K^{\text{relax}}$ seems more severe. However, one has to recall, that the g-value shift and the relaxation measure different averages of the exchange interaction.[6] It is common that usually

$$N(E_F)J^{\Delta g}\neq[N^2(E_F)\langle J^2(q)\rangle]^{1/2}\ .$$

If we assume a cutoff parameter of $D=10^2$ K, one yields[12]

$$[N(E_F)J]^{\Delta g}=-0.046$$

and

$$[N(E_F)J]^{\text{relax}}=-0.032\ .$$

In view of other ESR results this is a fair agreement.

IV. SUMMARY

This paper discusses the Kondo effect in the ESR of *Au*Yb for two isotopes, 171 and 174. Details of the experimental procedures were presented to show that the changes in the linewidth and the field for resonance are not due to interaction effects. Differences of the detailed resonances are explained by the field and frequency dependence of the relaxation rates. This can be shown unambiguously by the availability of three microwave setups in combination with a dilution refrigerator.

The theoretical analysis does explain the field and frequency dependence; however, the different T_K's remain as an unsatisfactory result. The reason for the discrepancy is the restrictive assumptions of our model Hamiltonian. We believe the main reason is the difference in the local-moment and CE g value. The theory in Ref. 9 is derived under the assumption of equal g values. Let us first compare the g-value shift of the former theory used in BT, Eq. (1), with the one[5] used in the present work, Eq. (3). For $h_0=0$ and $g=2$, both equations are identical. For $g\neq2$ in Eq. (1), one projects $\bar{S}$ on $\bar{J}$, yielding $\alpha=0.418$, and introduces $d=(2l+1)$ as a degeneracy parameter, whereas the present analysis does not introduce free parameters, only T_K remains to be fitted. Consequently, T_K will differ in both cases. More complicated but, in principle, similar arguments can be given for the relaxation rates. Table II shows the different fit results. A complete theory adaptable for *Au*Yb would have to treat local moment and CE with different eigenfrequencies ω_{loc} and ω_{CE}. Perturbation theory to third order then yields terms of the order of $\omega_{\text{CE}}\ln(kT/D)$ plus $(\omega_{\text{loc}}-\omega_{\text{CE}})\ln(kT/D)$. A proper calculation becomes very complicated and goes beyond the scope of the present investigation.

ACKNOWLEDGMENTS

We would like to thank B. Coqblin and S. E. Barnes for valuable discussions. The work was supported by the Deutsche Forschungsgemeinschaft (Sondersforschungsbereich 161). One of us (P.S.) acknowledges the receipt of a Heisenberg fellowship from the Deustche Forschungsgemeinschaft.

*Present address: Mechanical Engineering Department, University of South Alabama, Mobile, Alabama 36688.

[1]H. J. Spencer and S. Doniach, Phys. Rev. Lett. 18, 994 (1967).
[2]M. Loewenhaupt and W. Just, Phys. Lett. 53A, 305 (1975).
[3]P. Steiner, S. Hüfner, and W. V. Zdrojewski, Phys. Rev. B 10, 4704 (1974).
[4]H. Alloul, Physica 86-88B, 449 (1977); O. Kanert, M. Mali, K. Preusser, and M. Mehring, Solid State Commun. 21, 1047 (1977).
[5]W. Götze and P. Wölfle, J. Low Temp. Phys. 5, 575 (1971); W. Götze and P. Schlottmann, *ibid.* 16, 87 (1974).
[6]For details and notations see, R. Orbach, in *Proceedings of the Fourteenth International Conference on Low Temperature Physics, LT-14, Otaniemi, 1975,* edited by M. Krusius and M. Vuorio (Elsevier, New York, 1975), Vol. 5, p. 375.
[7]L. L. Hirst, G. Williams, D. Griffiths, and B. R. Coles, J. Appl. Phys. 39, 844 (1968).
[8]A. P. Murani, Solid State Commun. 12, 295 (1973).
[9](a) K. Baberschke and E. Tsang, Phys. Rev. Lett. 45, 1512 (1980); (b) E. Tsang and K. Baberschke, J. Appl. Phys. 52, 2208 (1981).
[10]J. Nagel, K. Baberschke and E. Tsang, J. Magn. Magn. Mater. 15-18, 1730 (1980).
[11]B. Hébral, K. Matho, J. M. Mignot, and R. Tournier, J. Phys. (Paris) Lett. 38, L347 (1977).
[12]A. K. Bhattacharjee and B. Coqblin, Solid State Commun. 18, 1587 (1976).
[13]Y. v. Spalden and K. Baberschke, J. Magn. Magn. Mater. 23, 183 (1981).
[14]M. E. Sjøstrand and G. Seidel, Phys. Rev. B 11, 3292 (1975).
[15]Y. v. Spalden and K. Baberschke, Physica 107B, 599 (1981).
[16]M. Peter, D. Shaltiel, J. H. Wernick, H. J. Williams, J. B. Mock, and R. C. Sherwood, Phys. Rev. 126, 1395 (1962).
[17]F. Dyson, Phys. Rev. 98, 349 (1955).
[18]H. Hacker, R. Gupta, and M. L. Shepherd, Phys. Status Solidi A 9, 601 (1972).

[19]K. Baberschke and Y. v. Spalden, Phys. Rev. B 19, 5933 (1979).
[20]F. Gonzalez-Jimenez and P. Imbert, Solid State Commun. 13, 85 (1973); F. Gonzalez-Jimenez, P. Imbert, and F. Hartmann-Boutron, Phys. Rev. B 9, 95 (1974).
[21]L. J. Tao, R. Orbach, and E. P. Chock, Phys. Rev. B 4, 5 (1971).
[22]P. W. Anderson, Commun. Solid State Phys. 1, 190 (1968).
[23]S. E. Barnes, J. Phys. F 6, 1713 (1976).
[24]D. Follstaedt and A. Narath, Phys. Rev. B 19, 1374 (1979).
[25]F. Gonzalez-Jimenez, B. Cornut, and B. Coqblin, Phys. Rev. B 11, 4674 (1975).
[26]B. Coqblin and J. R. Schrieffer, Phys. Rev. 185, 847 (1969).
[27]We use the following notation: $g_0\mu_B H \equiv h_0$, g_0 is the g value of the Γ_7 ground state; $g_0^{\text{theor}} = \frac{24}{7} \approx 3.429$ and g_0^{ionic} $(ThO_2) = 3.423$. For details, see Sec. IV. For $g\mu_B H' \equiv h$ we use $g_0 + \Delta g = g$.